JBC RESEARCH ARTICLE

Allosteric coupling between transmembrane segment 4 and the selectivity filter of TALK1 potassium channels regulates their gating by extracellular pH

Received for publication, December 24, 2021, and in revised form, April 19, 2022 Published, Papers in Press, April 29, 2022,
https://doi.org/10.1016/j.jbc.2022.101998

Wen-Hao Tsai (蔡文豪)[1,2,‡], Cédric Grauffel[1,‡], Ming-Yueh Huang (黃名鈺)[3], Sandra Postić[4], Marjan Slak Rupnik[4,5,6], Carmay Lim (林小喬)[1], and Shi-Bing Yang (楊世斌)[1,2,*]

From the [1]Institute of Biomedical Sciences, Academia Sinica, Taipei, Taiwan; [2]Taiwan International Graduate Program in Molecular Medicine, National Yang Ming Chiao Tung University and Academia Sinica, Taipei, Taiwan; [3]Institute of Statistical Science, Academia Sinica, Taipei, Taiwan; [4]Center for Physiology and Pharmacology, Medical University of Vienna, Vienna, Austria; [5]Institute of Physiology, Faculty of Medicine, University of Maribor, Maribor, Slovenia; [6]Alma Mater Europaea – European Center Maribor, Maribor, Slovenia

Edited by Mike Shipston

Opening of two-pore domain K^+ channels (K2Ps) is regulated by various external cues, such as pH, membrane tension, or temperature, which allosterically modulate the selectivity filter (SF) gate. However, how these cues cause conformational changes in the SF of some K2P channels remains unclear. Herein, we investigate the mechanisms by which extracellular pH affects gating in an alkaline-activated K2P channel, TALK1, using electrophysiology and molecular dynamics (MD) simulations. We show that R233, located at the N-terminal end of transmembrane segment 4, is the primary pH_o sensor. This residue distally regulates the orientation of the carbonyl group at the S1 potassium-binding site through an interacting network composed of residues on transmembrane segment 4, the pore helix domain 1, and the SF. Moreover, in the presence of divalent cations, we found the acidic pH-activated R233E mutant recapitulates the network interactions of protonated R233. Intriguingly, our data further suggested stochastic coupling between R233 and the SF gate, which can be described by an allosteric gating model. We propose that this allosteric model could predict the hybrid pH sensitivity in heterodimeric channels with alkaline-activated and acidic-activated K2P subunits.

In potassium (K^+) channels, the K^+ ions pass through pore regions assembled from tetrameric pore-forming sequences, including the pore helix (PH) and the selectivity filter (SF; amino acid sequence, T-V/I-G-F/Y-G). The PH provides a supporting force to maintain the conformation of the SF, while the five carbonyl groups in the SF form the K^+ binding sites (S0-S4) that mimic K^+ hydration (1, 2). Mild distortion of the SF conformation destabilizes K^+ binding in ways that can tremendously impact the channel properties, including opening probability (P_o), conductance, and gating kinetics (3–7). This phenomenon has been demonstrated as the molecular basis of SF gating, that is, C-type gating, in potassium channels (8).

Two-pore domain K^+ (K2P) channels (Fig. 1*A*) are a group of dimeric proteins responsible for setting the resting membrane potentials of various cell types (9–11). These channels are responsive to diverse external cues such as pH (12), membrane tension (13–15), and temperature (16, 17), which are widely thought to regulate K2P activities via C-type gating mechanisms. However, the cue-sensing residues are clustered in a hot-spot region formed by the M1P1 loop, the M2P4 loop, and the N-terminal or C-terminal portions of transmembrane segment 4 (TM4), which is structurally far from the SF (18–21). Therefore, the molecular linkages between the cue sensors and C-type gates are not immediately apparent and must be defined for each type of K2P channel.

Extracellular pH (pH_o) regulates the C-type gate in three subtypes of K2P channels, including the TWIK-related acid-sensitive K^+ channel (TASK), TWIK-related K^+ channel (TREK), and TWIK-related alkaline pH-activated K^+ channel (TALK) families. A set of crystallographic studies for TREK1 showed that the K^+-dependent C-type gating involves disruption of S1 and S2 ion binding via asymmetric rearrangements of the backbone of SF1 and SF2 (22). Of note, heterodimeric TREK1 and TREK2 show a hybrid pH_o sensitivity that can be activated by both acidification and alkalinization (23–25). In TASK3, a protonated H98 at the mouth of the SF guards the narrow entrance of side portals toward the S0 binding site (26). Compared to other pH_o-operated K2P channels, TALK channels are activated at relatively high pH_o (12). Previous studies suggested that this property may be due to high-pK_a basic residues such as Arg and Lys in the TM4 acting as the pH_o sensor (20, 27). Furthermore, a recently released structure for TASK2 suggested that a protonated Arg causes dilation of the S1 and S0 sites of SF1 through interaction with E228 and rearrangement of the long extracellular M1P1 loop (28). Although the TALK1 channel has a conserved Arg (R233), it lacks a Glu at the position equivalent to TASK2-E228 (i.e., TALK1-A237). Additionally, the low similarity between the M1P1 loops of TASK2 and TALK1 (Fig. 1*B*) suggests that TALK1 may exhibit a different pH_o gating

‡ These authors contributed equally to this work.
* For correspondence: Shi-Bing Yang, sbyang@ibms.sinica.edu.tw.

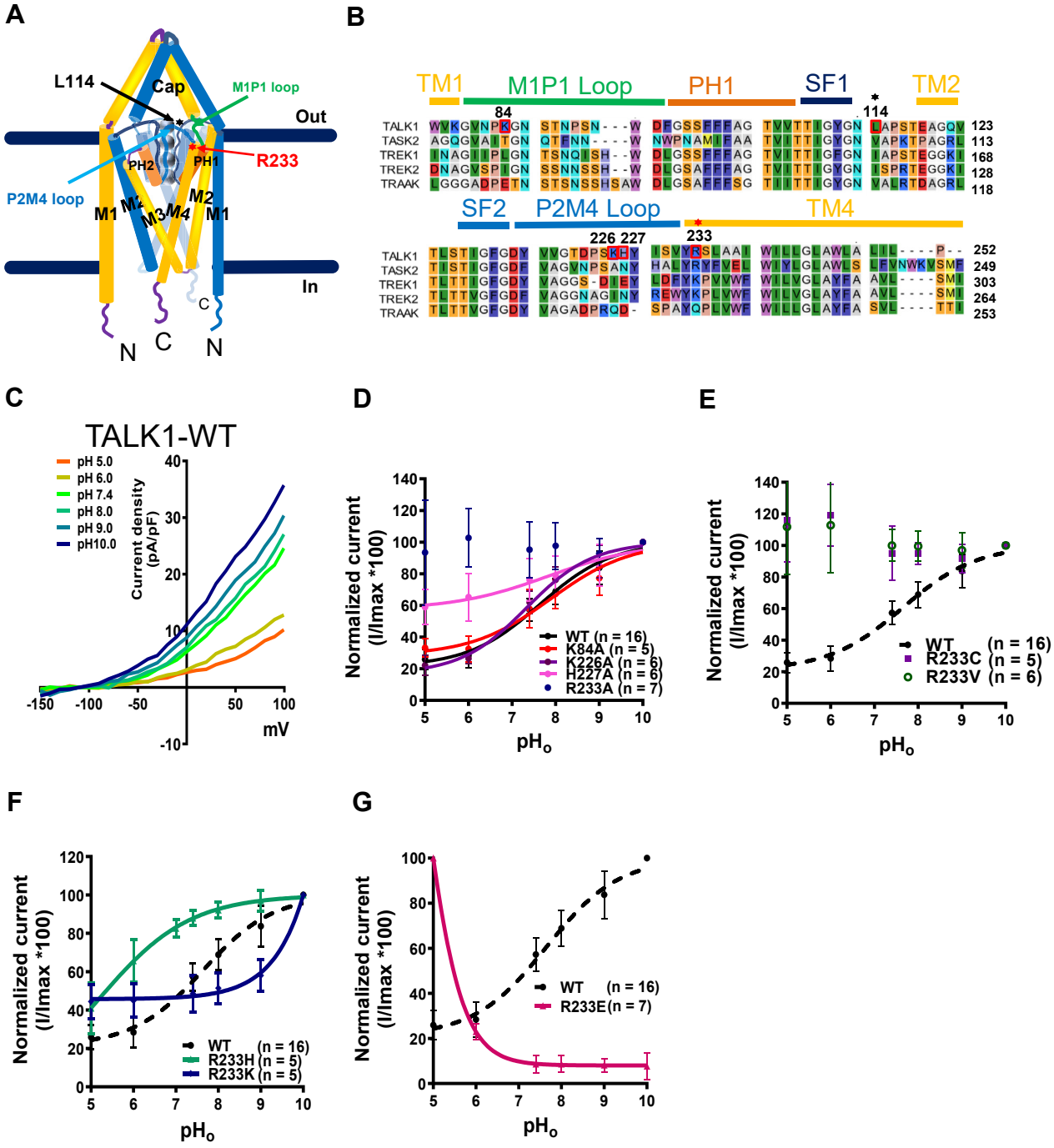

Figure 1. R233 is the primary pHo sensor of TALK1. *A*, the diagram represents the domain-swapping architecture of the TALK1 channel. *Blue* and *yellow* colors represent individual TALK1 subunits; *white spheres* represent K^+. The M1P1 loop and P2M4 loop are highlighted in *green* and *blue*, respectively. TM1-TM4 are labeled as M1-M4 in the diagram. *B*, the amino acid sequence alignment of the M1P1 loop, PH1, P2M4 loop, and TM4 regions among pH_o-sensitive K2P channels, including TALK1 (NP_001128578), TASK2 (NP_003731), TREK1 (NP_001017424), TREK2 (XP_024305396), and TRAAK (NP_201567). The *dashed line* represents missing residues. *Red squares* represent the four pH_o sensor candidates in TALK1, K84, K226, H227, and R233. The critical residues R233 and L114 are labeled by *red* and *black asterisks* in (A) diagram and (B) sequence alignment, respectively. *C*, the I-V plot shows the whole-cell currents from COS7 cells transfected with WT TALK1 channels at various pH_o values (pH_o 5.0 − 10.0); the external and internal solutions contain 2 mM K^+ and 150 mM K^+ (E_K = −110 mV), respectively. *D*, the pH_o-sensitive curves of four candidates were acquired by normalizing to the current densities at pH_o 10.0, 0 mV, and by fitting with the Hill equation. Two parameters, $pK_{1/2}$ and nH, reveal the pH_o sensitivity of TALK1-WT ($pK_{1/2}$ = 7.6 ± 0.1; nH = 0.52 ± 0.05, n = 16), K84A ($pK_{1/2}$ = 7.9 ± 0.2; nH = 0.48 ± 0.10, n = 5), K226A ($pK_{1/2}$ = 7.3 ± 0.1; nH = 0.57 ± 0.08, n = 6), H227A ($pK_{1/2}$ = 7.8 ± 0.6; nH = 0.40 ± 0.18, n = 6), and R233A (unsuccessful fitting, n = 7). The pH_o-sensitive curves represent pH_o sensitivities of (E) neutral, (F) positively charged, and (G) negatively charged residues at position 233. The *black dashed lines* represent TALK1-WT from Figure 1*D* (n = 5 for R233V and 6 for R233C, respectively); both pH_o-sensitive curves cannot be fitted with the Hill equation. The $pK_{1/2}$ of R233H is 5.2 ± 1.1 and nH is 0.41 ± 0.08 (n = 5); the $pK_{1/2}$ of R233K is >10 (n = 5). The negatively charged R233E exhibits acidic activation (n = 7). K2P, two-pore domain potassium channel; PH, pore helix; TASK, TWIK-related acid-sensitive K+ channel; TM, transmembrane region; TREK, TWIK-related K+ channel.

mechanism than TASK2. Interestingly, a recent case report showed that a novel TALK1 mutant, L114P, causes maturity-onset diabetes of the young (29). TALK1 is abundantly expressed in the pancreatic β cells (9, 30), and this gain-of-function L114P mutation was shown to inhibit glucose-stimulated insulin secretion (29). Since L114 is located near the outer mouth of the SF (Fig. 1*A*), it is likely to be involved in C-type gating. While these studies provide key pieces of information about the TALK1 gating mechanism, a comprehensive model has not been developed.

In this study, we investigated the mechanisms of pH_o sensitivity in TALK1 channels by combining mutagenesis, electrophysiology, and molecular dynamics (MD) simulations. Based on our findings, we generated a model to describe the allosteric mechanisms of pH_o gating in TALK1. Briefly, we found that the peripheral sensor, R233, stochastically regulates the C-type gate by flipping the carbonyl group of the S1 K^+-binding site in SF1. Our model further predicts the behavior of heterodimeric R233 mutants, especially for the hybrid activation of heterodimeric K2P channels comprised of channel subtypes with distinct gating properties.

Results

R233 is the pH_o-sensing residue in TALK1

To investigate the pH_o-sensitivity of TALK1, we transfected pCDNA3.1 hTALK1 variant 3 into COS-7 cells and recorded whole-cell currents under a range of pH_o values (pH_o 5–10). The current-voltage plot of TALK1 WT showed typical outward-rectification under 2 mM $[K^+]_o$/150 mM $[K^+]_i$, and the currents were augmented by alkaline conditions with a $pK_{1/2}$ of 7.6 ± 0.1 and Hill coefficient (nH) of 0.52 ± 0.05 (Fig. 1, *C* and *D*) (9). For other pH_o-sensitive K2P channels, a single basic amino acid located either at the M1P1 loop, P2M4 loop, or the N-terminal TM4 domain has been shown to be the pH_o sensor (18–20, 28). Sequence alignment of these pH_o-sensitive K2P channels suggested four candidate pH_o sensors, K84, K226, H227, and R233 (Fig. 1*B*). To evaluate whether any of these basic residues is the TALK1 pH_o sensor, we mutated each residue to Ala and examined the resultant pH_o sensitivities.

All the mutant channels exhibited stereotypical outward-rectification under 2 mM $[K^+]_o$/150 mM $[K^+]_i$ (Fig. S1, *A*–*D*). Moreover, the TALK1-K84A and K226A mutants displayed comparable alkaline activation characteristics. The K84A mutant exhibited a $pK_{1/2}$ of 7.9 ± 0.2 and nH of 0.48 ± 0.10, while the K226A mutant had a $pK_{1/2}$ of 7.3 ± 0.1 and nH of 0.57 ± 0.08 (Fig. 1*D*, red and purple curves). Although the TALK1-H227A mutant also displayed alkaline activation, with $pK_{1/2}$ of 7.8 ± 0.6 and nH of 0.40 ± 0.20, its span of current intensity was significantly reduced (Fig. 1*D*, magenta curve). By contrast, although the TALK1-R233A exhibited comparable current densities as the WT, its pH_o sensitivity was completely abolished (Fig. 1*D*, blue circle). This result strongly suggests that R233 is the principal pH_o sensor. Substituting R233 with other neutral amino acids such as Cys or Val also abolished the pH_o sensitivity (Fig. 1*E*). Moreover, conservative mutation preserved the pH_o sensitivity, as the $pK_{1/2}$ values were 5.16 ± 1.17 for R233H and > 10 for R233K, which are close to the pK_a for His (6.0) and Lys (10.5), respectively (Fig. 1*F*). Interestingly, the TALK1 R233E mutant displayed acidic activation rather than alkaline activation (Fig. 1*G*).

R233 protonation triggers flipping of the K^+-ligating carbonyl group at the S1 site

Since R233 is located at the N-terminal part of TM4, far from the K^+ permeation pathway (Fig. 1*A*), it cannot directly block K^+ flow via electrostatic repulsion, as demonstrated for the pH_o-sensing mechanism of TASK3 (26). To investigate how R233 might control the pH_o sensitivity of TALK1, we compared MD simulations of protonated R233 ($R233^+$) and deprotonated R233 ($R233^0$). The dihedral angles of the ^{108}T-I-G-Y-G^{112} residues lining the SF displayed greater variability in the MD simulations for $R223^+$ than those for $R233^0$. In particular, the backbone dihedral of Y111 lining the SF (Ψ_{Y111}) rotated by ∼180° in 20% (replicates 1, 8, 11, and 16) of the $R233^+$ simulations (Fig. 2*A*, top left and S2A), but this phenomenon was absent in the $R223^0$ simulations (Fig. 2*A*, top right and S2B). This flip coincided with the loss of coordination between the Y111 carbonyl oxygen and K^+ at the S1 binding site (Fig. 2*B*). Of note, the Ψ angle of I109 at the S3 binding site was also highly dynamic, but there was no observable difference in this angle between the $R233^0$ and $R233^+$ simulations (Fig. 2*A*, bottom panel). Therefore, although there are two locations (S1 and S3) in TALK1 that may contribute to C-type gating, only S1 is likely to be dependent on the protonation status of R233.

The pH_o-dependent C-type gating of TASK2 involves the dilation of the S0 and S1 K^+ binding sites in SF1 (28). Additionally, the kinetics of voltage-dependent K2P channels involves a slow rearrangement of the SF (31, 32). Such a slow rearrangement differs from the rapid flipping of the carbonyl groups of the K^+ binding sites (4–6). Moreover, an alkaline extracellular solution would be expected to expedite the voltage-dependent process, but it may not affect the rapid gating by flipping the carbonyl group. As expected, elevating pH_o accelerated the voltage-dependent activation of the TASK2-WT (48.41 ± 17.14 ms at pH_o 7.4, 21.80 ± 10.44 ms at pH_o 9.0) but not the pH_o-insensitive TASK2-R224A mutant (41.57 ± 5.81 ms at pH_o 7.4, 34.90 ± 8.07 ms at pH_o 9.0) (Figs. S3, *A* and *B*, 2*E*). By contrast, varying pH_o had no effect on the voltage-dependent activation of either pH_o-sensitive TALK1-WT (0.19 ± 0.11 ms at pH_o 7.4, 0.44 ± 0.73 ms at pH_o 9.0) or pH_o-insensitive TALK1-R233A (2.97 ± 1.65 ms at pH_o 7.4, 3.04 ± 2.1 ms at pH_o 9.0) (Fig. 2, *C*–*E*). These results imply that TALK1 and TASK2 may utilize distinct gating mechanisms even though

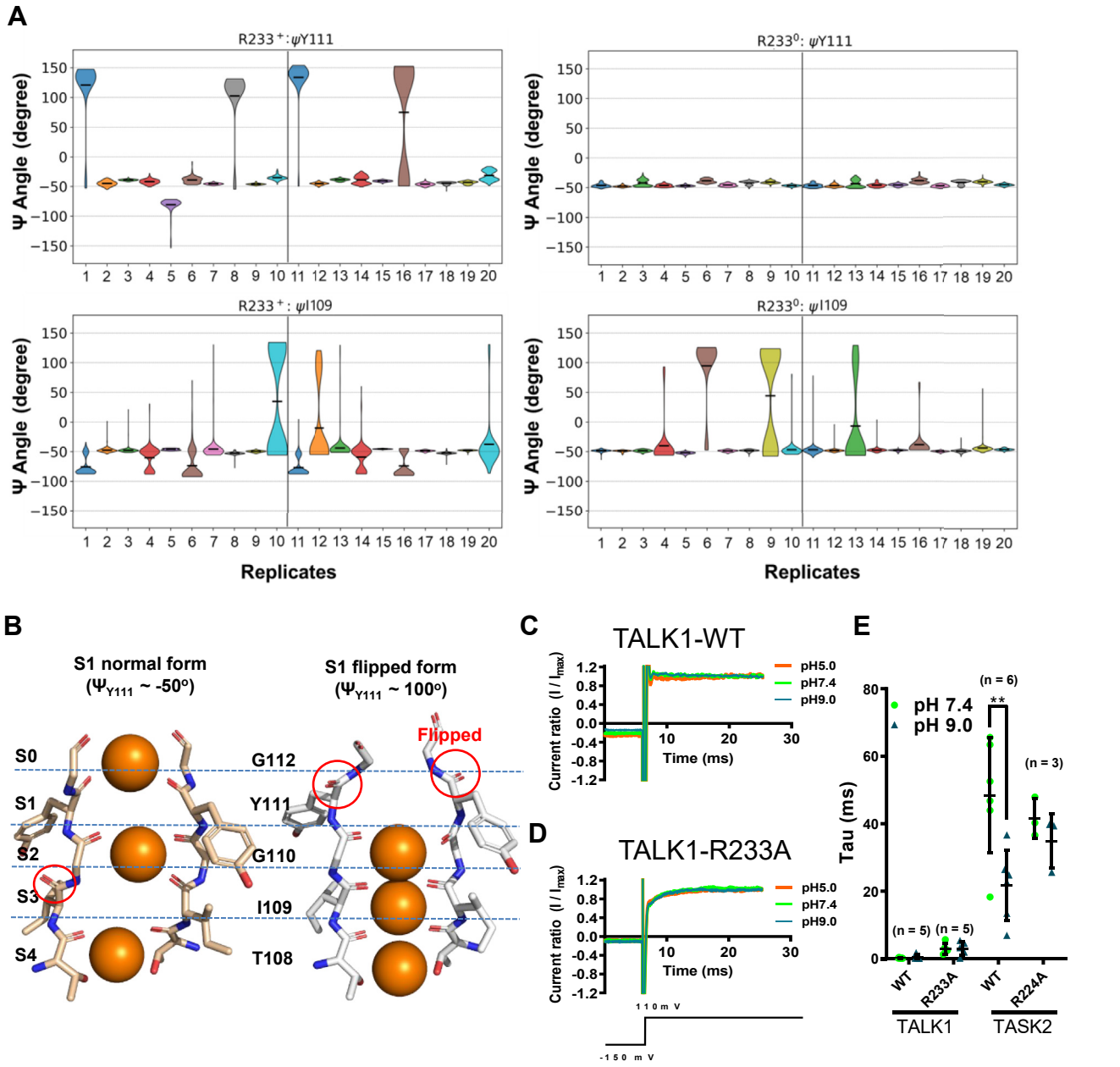

Figure 2. The carbonyl group at S1 K+ binding site is often flipped in R233+ MD simulations. *A*, the violin plots show the $C_\alpha\Psi$ angle of Y111 (S1 K^+-binding site) and I109 (S3 K^+-binding site) during $R233^0$ or $R233^+$ MD simulations. For each condition, ten sets of 200 ns MD simulations were performed; each column represents a single run of MD simulation for individual subunits (1–10 for subunit 1 and 11–20 for subunit 2). The *black bars* represent the average angles during each simulation. *B*, representative snapshots of the S1 K^+-binding site from an $R233^+$ simulation. The Y111 backbone carbonyl oxygen was either pointing toward (*left*, $\Psi_{Y111} \sim -50°$) or away (*right*, $\Psi_{Y111} \sim 100°$) from the S1 K^+-binding site. The *orange spheres* represent K^+. Normalized TALK1 currents from (C) TALK1-WT and (D) R233A upon a voltage step from -150 mV to 110 mV at a different pH_o. *E*, the average time constants (τ) of voltage-dependent activation of TALK1 or TASK2 mutants were acquired by fitting with a single exponential equation: $f(t) = A(1\text{-}e^{(-t/\tau)}) + C$. The alkaline solution accelerated the voltage-dependent activation in WT TASK2 but not TALK1. Neutralizing the pH_o sensor (TASK2 R224A) also abolished the voltage-dependent activation (**$p < 0.01$, paired *t* test). TASK, TWIK-related acid-sensitive K+ channel.

their pH_o sensors and corresponding gates are located at the equivalent position.

The interaction network of R233, PH1, and SF regulates C-type gate

Comparison of the structures between S1 normal and flipped forms shows that the side chains of R233 (at the TM4 N-terminus) and L114 (positioned halfway between the R233 and the SF) were rotated (Fig. 3*A*), suggesting extensive interactions might connect R233 at TM4 to L114 near the SF. To test this hypothesis, we examined the interaction partners of R233 and L114 during the $R233^0$ and $R233^+$ simulations.

The positively charged $R233^+$ side chain did not have a stable partner during the $R233^+$ simulations; its most stable hydrogen bond was with the S97 side chain, which occurred in only 20 to 30% of the total simulation time (Fig. 3*B*). In the presence of the $R233^+$/S97 hydrogen bond, $R233^+$ rotated toward the L114 side

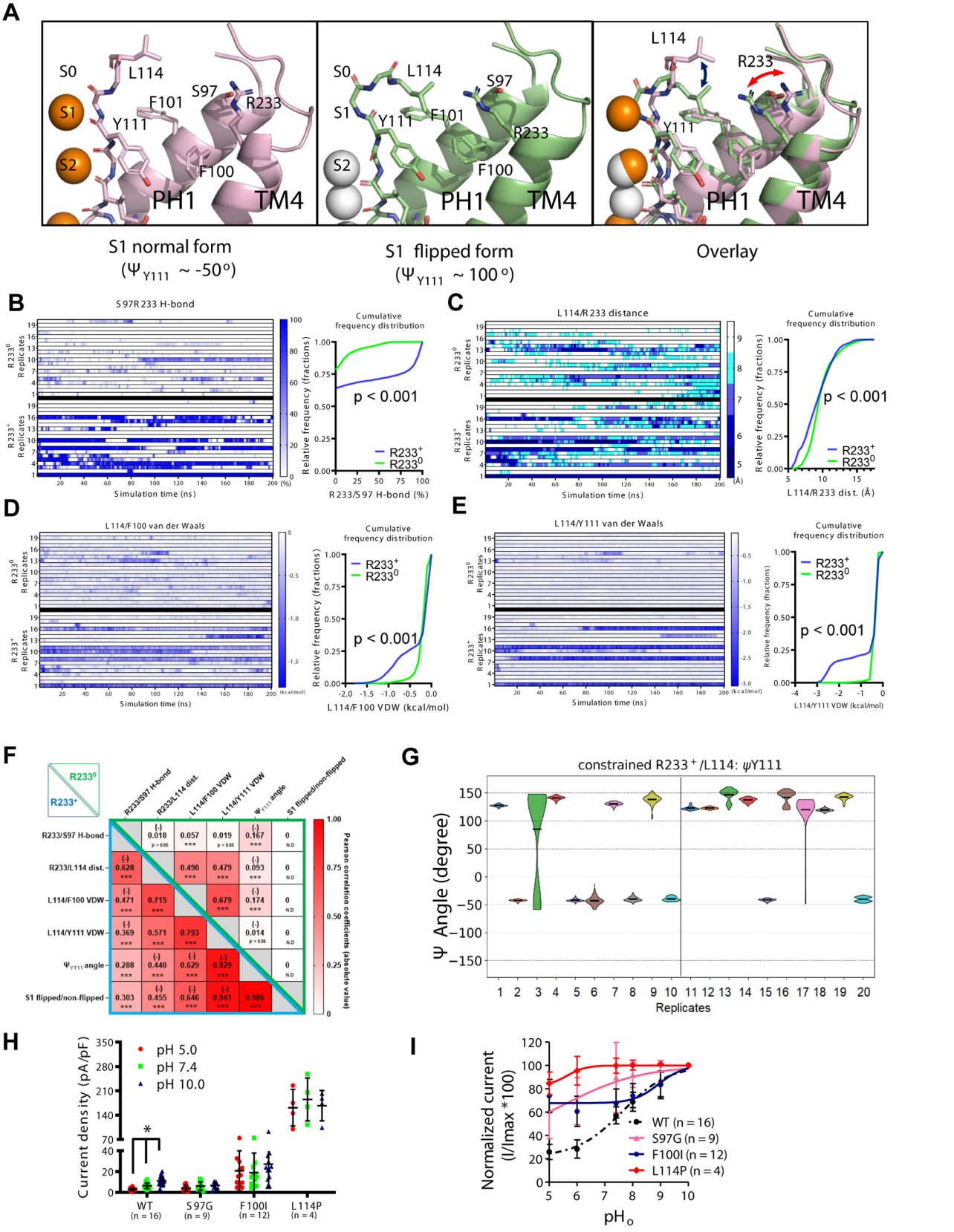

Figure 3. Interaction network among R233, PH1, and SF determines the pHo sensitivity of TALK1. *A*, the diagrams represent conformational change between normal and flipped R233$^+$, and the *white* and *orange* spheres represent K$^+$. *B–E*, summary of the interaction strengths between critical residues from R233$^+$ and R233^0 simulations. Ten independent sets of 200-ns MD simulations were performed: replicate 1 to 10 for subunit one and replicate 11 to 20 for subunit two. *B*, R233/S97 hydrogen-bond interaction (in %). *C*, R233/L114 distance (in Å) van der Waals interaction energy (in kcal/mol) between F100 and L114 (D) or Y111 and L114 (E). The cumulative frequency distributions for each interaction were analyzed by the Kolmogorov–Smirnov test. *F*, the Heat

chain ($R233^+$/L114 distance ~ 5.5 – 6.5 Å in Figs. 3*C* and S2*A*, Pearson coefficient = –0.628, Fig. 3*F*). We noticed that sometimes, but not always, the shortening of the $R233^+$/L114 distance preceded the Ψ_{Y111} rotation (Fig. S2*A*, flipped; replicate 5, 6, 7,10 and 14 in non-flipped), implying the $R233^+$-induced Ψ_{Y111} rotation is a stochastic process. Moreover, we also observed stronger van der Waals interactions for L114/F100 (-1.5 to -1.0 kcal/mol, Figs. 3*D* and S2*A*) and L114/Y111 (–2.0 to –2.5, Figs. 3*E* and S2*A*) in the closed conformation (S1 flipped). These stable van der Waals interactions of L114/F100 and L114/Y111 only occurred after the Ψ_{Y111} shifted to ~100^0 (Fig. S2*A*, flipped), suggesting a strong coupling between Y111/L114/F100 and the Ψ_{Y111} rotation (Fig. 3*F*). In contrast, $R233^0$ occasionally formed a hydrogen bond with the backbone of V220 (occupancy of 37%) but the interactions with S97 became unstable (occupancy of 5%) (Figs. 3*B* and S2*B*). Most importantly, in all $R233^0$ simulation replicates, R233 never came in close contact with L114 ($R233^+$/L114 distance > 6.5 Å, Figs. 3*C* and S2*B*), and the F100-L114-Y111 interactions that linked the SF to R233 became infrequent (Figs. 3, *D* and *E*, S2*B*). Overall, these observations suggest that multiple transient interactions connect $R233^+$ to the conformational changes of the S1 binding site.

To further establish a dynamic link between $R233^+$ and the SF, we carried out a series of simulations in which the R233-C_ζ and L114-C_γ distance was constrained to the shortest observed in the unconstrained simulations ($R233(C_\zeta)$—$L114(C_\gamma)$ = 5.3 Å). In agreement with our hypothesis, we observed more frequent rotation of Ψ_{Y111} in these simulations (13/20, 65%) as compared with unconstrained $R233^+$ simulations (Fig. 2*A*, top left and 3G; 4/20, $p < 0.01$, Fisher's exact test).

To confirm the predicted role of the R223–PH1-L114 interaction in channel activation, we generated S97G, F100I, and L114P mutants and examined their pH_o sensitivities. As expected, TALK1-S97G had an attenuated activation at high pH_o and an acidic-shifted $pK_{1/2}$ (Fig. 3, *H* and *I*). TALK1-F100I exhibited weakened proton inhibition with elevated current densities (Fig. 3, *H* and *I*). The electrophysiological recording of TALK1-L114P mutants revealed a disruption of pH_o sensitivity and a 15-fold increase in current density (Fig. 3, *H* and *I*), in agreement with the previous study (29).

R233E reverses pH$_o$ sensitivity by establishing PH1 and M1P1 loop interaction networks in the presence of divalent cations

In contrast to positively charged Arg, Glu is a negatively charged at physiological pH; therefore, we predicted that the R233E mutation would exhibit different sensitivity to pH_o. Indeed, TALK1-R233E showed an acidic activation (Fig. 1*G*). Based on the modeled structure of R233E, we then hypothesized that residues R233E, D94, and S97 could form a binding pocket for divalent cations (dications) such as Ca^{2+} and Mg^{2+}, which would inhibit TALK1-R233E currents in alkaline conditions ($pH_o > 5.0$), mimicking $R233^+$ (Fig. 4*A*). To test this hypothesis, we recorded TALK1-WT and TALK1-R233E currents in a dication-free extracellular solution (Ca^{2+} and Mg^{2+}-free plus 1 mM EDTA, pH 7.4). This dication-free solution at pH_o 7.4 could activate TALK1 R233E (fold increase =16.23 ± 9.15, n = 9) but not WT (fold increase =1.12 ± 0.84, n = 6) (Fig. 4, *B* and *C*). Furthermore, although both Ca^{2+} and Mg^{2+} could inhibit TALK1-R233E, Ca^{2+} was twice as potent as that of Mg^{2+} at the same concentration (1 mM) (Fig. S4, *A*–*E*).

To further test our hypothesis, we examined the acidic activation of a double mutation, R233E + D94A. If D94 is involved in the acidic activation of the R233E mutant, this double mutant could abolish this acidic activation. We first confirmed that D94A single mutant exhibited normal pH_o sensitivity (Fig. S4*F*). As expected, acidic activation was lost in TALK1-R233E + D94A (Fig. 4*D*). This result further suggested that R233E and D94 could form a dication-binding pocket. We then tested the ability of these acidic residues to capture a Ca^{2+} by creating three different starting conformations for MD simulations of the TALK1-R233E mutant in which a Ca^{2+} ion was placed close to either E233 or D94. These simulations revealed that Ca^{2+} tightly bound the carboxylates of E233 and D94. S97 could also coordinate Ca^{2+}, but the interaction was more sporadic (Fig. S4*G*). Therefore, inhibition of TALK1-R233E at high pH_o might result from a mimicking of the $R233^+$–PH1 interaction.

Allosteric pH$_o$-gating model for TALK1

Together, the electrophysiological experiments and MD simulations suggested an allosteric pH_o-gating model for TALK1 (Fig. 5*A*). We proposed that the protomeric TALK1 can adopt various conformations, including $R233^0$ (P1), $R233^+$ with normal SF (P2), and $R233^+$ with flipped SF (C). Both P1 and P2 represent K^+-permeable conformations, whereas the C represents a nonconductive conformation. At low pH_o, the $R233^0$ (P1) will be protonated ($R233^+$). $K_D{}^n$ represents the proton dissociation constant of R233, and n denotes proton sensitivity. Because $R233^+$ does not always induce a conformational change in the SF, we included a stochastic component α, an equilibrium constant between normal and flipped SF. Based on our model (Fig. 5*A*), the K^+ permeation probability (P_p) of protomer can be calculated by

$$P_p = \frac{1+\left(\frac{[H^+]}{K_D}\right)^n}{1+\left(\frac{[H^+]}{K_D}\right)^n+\alpha\left(\frac{[H^+]}{K_D}\right)^n} \quad (1)$$

where $[H^+]$ denotes the concentration of protons. Since a

map illustrates the Pearson correlation coefficient between various parameters including R233/S97 H-bond, R233/L114 distance, L114/F100 and L114/Y111 van der Waals interaction, Ψ_{Y111} angle, and S1 flipped/non-flipped in the $R233^+$ and $R233^0$ simulations (***$p < 0.001$, Pearson correlation analysis). The flipped and non-flipped S1 were defined as 1 and -1, respectively. The correlation coefficients were presented as the absolute value, and the negative correlation was labeled with (-). Since we did not observe the flipped S1 in $R233^0$ simulations, the correlation coefficients of S1 flipped/non-flipped in $R233^0$ with other factors cannot be determined. *G*, the violin plots of the $C_\alpha\Psi$ angle (Y111) when the R233/L114 distance was set at 5.3 Å. Ten sets of 100-ns MD simulations were conducted; each column represents one replicate of MD simulations for individual subunits (1–10 for subunit 1 and 11–20 for subunit2). The *black bars* represent the average angles during the whole simulation. *H*, the current densities at 0 mV of COS7 cells transfected with TALK1 S97G, F100I, or L114P mutants at different pH_o (*$p < 0.05$, 2-way ANOVA). *I*, the normalized pH_o-sensitive curves for S97G, F100I, and L114P mutants. The results for TALK1-WT (*dash line*) are from Figure 1*D*. PH, pore helix; SF, selectivity filter.

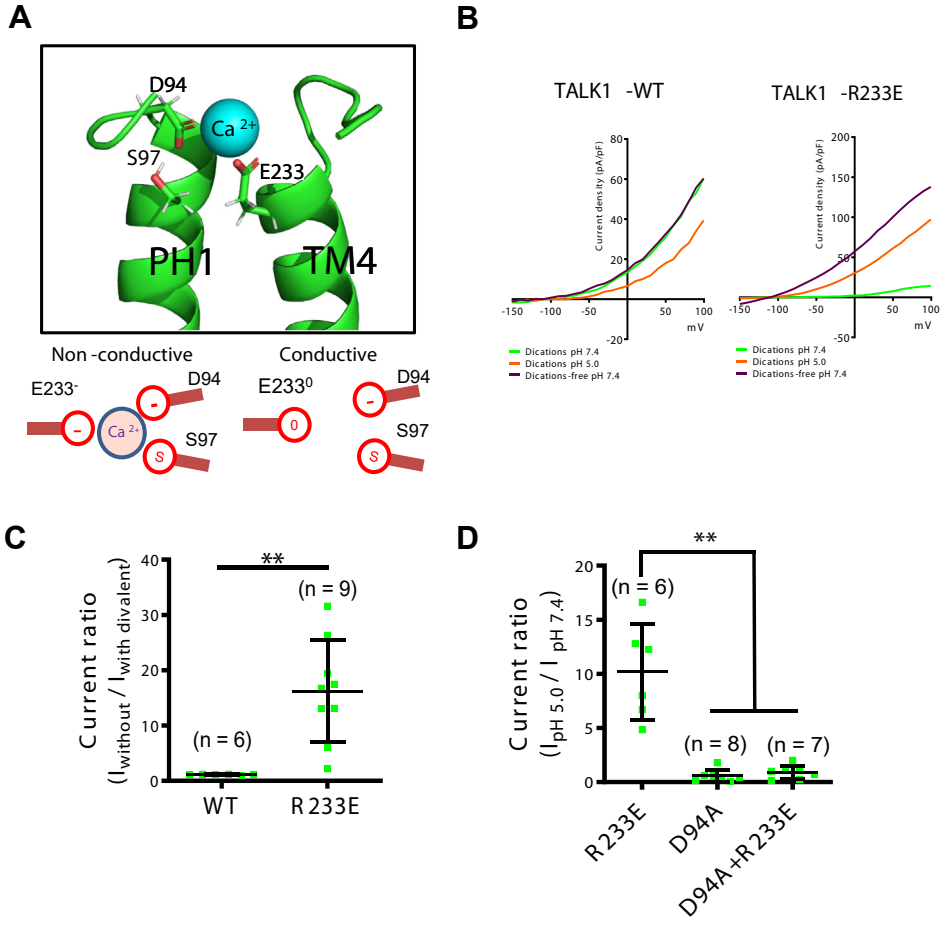

Figure 4. Dications inhibit TALK-R233E channels by mimicking interaction networks between R233 and PH1. *A*, the diagram illustrates the dication binding pocket formed by E233, D94, and S97 and the interacting partners of R233E with or without the Ca^{2+}. *B*, sample traces of TALK1 WT and R233E recorded with or without dications. *C*, the normalized current amplitudes for TALK1-WT (n = 6) or R233E (n = 9) (**$p < 0.01$, Student's test). *D*, the current ratios of $I_{pH\ 5.0}/I_{pH\ 7.4}$ for TALK1-R233E (n = 6), D94A (n = 8), or R233E D94A double mutants (n = 7). (**$p < 0.01$, One-way-ANOVA). PH, pore helix.

functional TALK1 channel is a dimer, the pH_o-dependent P_o relative to pH_o 10 can be calculated by

$$\frac{P_o}{P_o(pH\ 10)} = \left(\frac{1+\left(\frac{[H^+]}{K_D}\right)^n}{1+\left(\frac{[H^+]}{K_D}\right)^n+\alpha\left(\frac{[H^+]}{K_D}\right)^n}\right)^2 \Bigg/ \left(\frac{1+\left(\frac{10^{-10}}{K_D}\right)^n}{1+\left(\frac{10^{-10}}{K_D}\right)^n+\alpha\left(\frac{10^{-10}}{K_D}\right)^n}\right)^2 \quad (2)$$

Here, we assume that the protonation of R233 in one subunit is independent of protonation in the other subunit due to the distance between residues.

We then refitted the pH_o sensitivity curve of TALK1-WT with Equation 2 (Fig. 5*B*) and obtained values for the parameters α, pK_D, and n (Table 1). We found a mild acidic shift of pK_D compared to $pK_{1/2}$ estimated by the Hill equation. Also, the value of n was slightly smaller than that of nH. Of note, the value of α would yield a residual current around 15% at the extreme low pH_o. This value is considered to be the TALK1 residual current that has been reported previously (33).

Next, we established a similar model for TALK1-R233E (Fig. S5*A*). Its pH_o-dependent open probability ($P_{o(E)}$) relative to pH_o 5 can be calculated by

$$\frac{P_{o(E)}}{P_o(E,pH\ 5)} = \left(\frac{1+\left(\frac{[H^+]}{K_{D(E)}}\right)^{n(E)}}{1+\left(\frac{[H^+]}{K_{D(E)}}\right)^{n(E)}+\alpha_E}\right)^2 \Bigg/ \left(\frac{1+\left(\frac{10^{-5}}{K_{D(E)}}\right)^{n(E)}}{1+\left(\frac{10^{-5}}{K_{D(E)}}\right)^{n(E)}+\alpha_E}\right)^2 \quad (3)$$

where $K_{D(E)}{}^n$ represents the proton dissociation constant of R233E, α_E denotes the equilibrium constant between normal

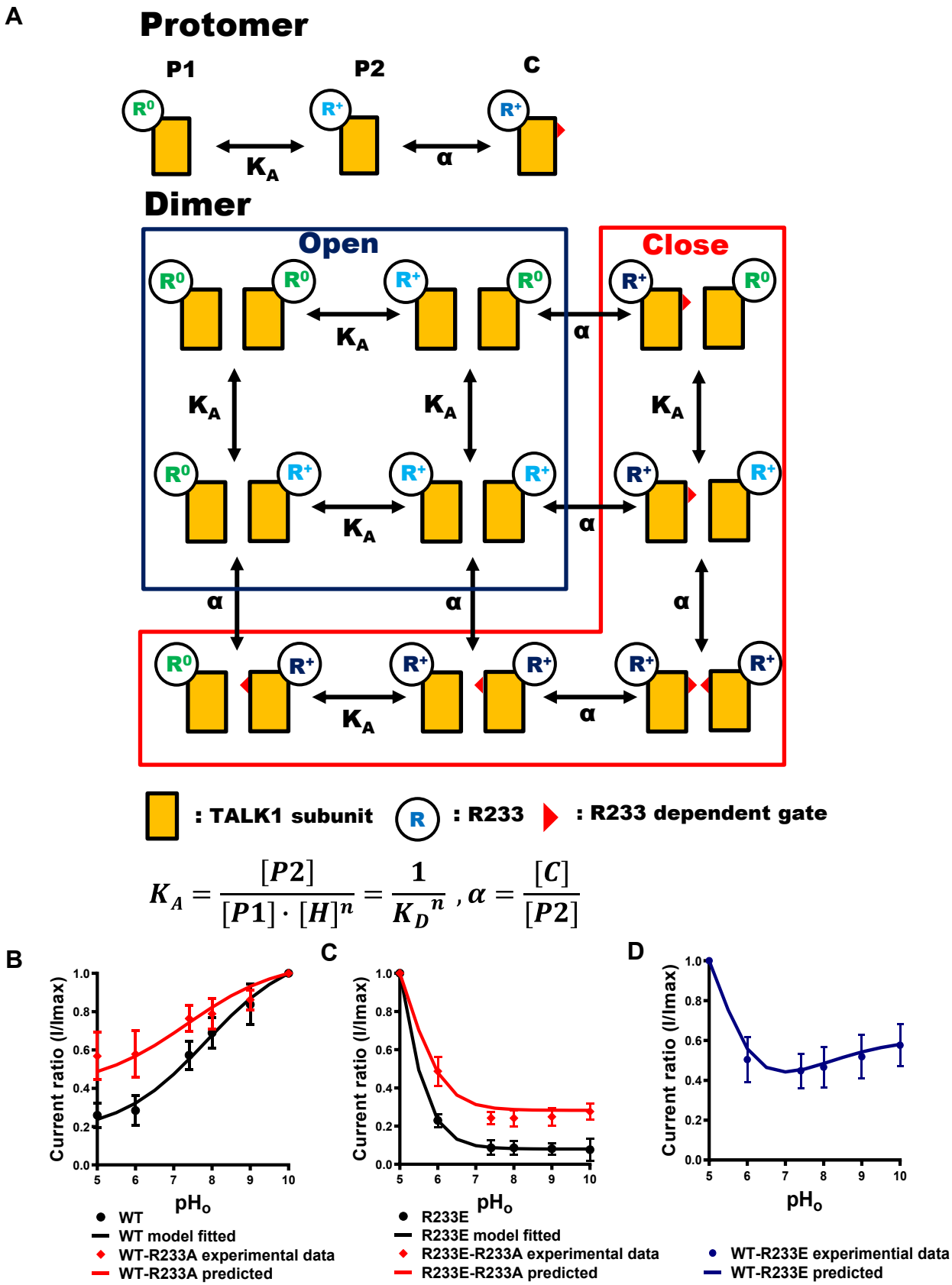

Figure 5. The pHo-dependent allosteric gating model for TALK1. *A*, the gating models for the promoter and the dimer. P1 and P2 represent the K^+ permeable forms; C represents the nonconductive form (S1 K^+-binding site flipped). The open and closed states of a dimer follow a binomial distribution. *B–D*, the current ratio plots show experimental (*dot*) and predicted (*line*) pH_o-sensitivities of various heterodimers, including (*B*) WT-R233A, (*C*) R233E-R233A, and (*D*) WT-R233E. The results of (B) WT and (C) R233E were fitted with Equations 2 and 3, respectively. The *red line* represents predicted pH_o activation of

Table 1
Parameters of pH_o-dependent allosteric gating model for TALK1 WT and R233E

Parameters	WT	R233E
α	1.64	4.27
pK_D	6.18	6.01
n	0.36	0.88

All parameter values were acquired by fitting the data from Figure 1, *D* and *G* with Equations 2 and 3, respectively. The fittings were conducted using R software.

and flipped SF when R233E is deprotonated ($R233E^-$), and $n_{(E)}$ denotes the proton sensitivity. It is worth noting that the value of α_E was dependent on the presence or absence of dications. Because glutamate has a negatively charged side chain, Equation 3 has minor differences from Equation 2. Refitting the pH_o sensitivities of TALK1-R233E with Equation 3 (Fig. 5*C*), we found that the residual current of TALK1-R233E dropped to only 7.9%.

The pH_o sensitivities of heterodimeric TALK1 R233 mutants can be predicted by the allosteric pH_o-gating model

A key feature of the allosteric pH_o-gating model is independent gating for each protomer. Thus, we hypothesized that the pH_o sensitivities of heterodimeric TALK1 R233 mutants, for example, WT-R233A, R233E-R233A, and WT-R233, could be predicted by the product of the P_p for each subunit, that is, $P_{o(subunit1-subunit2)} = P_{p(subunit1)} \times P_{p(subunit2)}$. The former term represents the pH_o-dependent P_p of subunit 1, and the latter term represents the pH_o-dependent P_p of subunit 2. The pH_o-dependent P_p of TALK1-WT is given by Equation 1. Since TALK1-R233A is pH_o-insensitive, its pH_o-dependent P_p is set to 1. Furthermore, the pH_o-dependent P_p of TALK1-R233E is

$$P_{p(E)} = \frac{1+\left(\frac{[H^+]}{K_{D(E)}}\right)^{n(E)}}{1+\left(\frac{[H^+]}{K_{D(E)}}\right)^{n(E)}+\alpha_E} \quad (4)$$

As an example, the pH_o sensitivity of heterodimeric TALK1-R233E-R233A relative to pH_o 5 could be predicted by

$$\frac{P_{o(R233E-R233A)}}{P_o(pH\ 5)} = \left(\frac{1+\left(\frac{[H^+]}{K_{D(E)}}\right)^{n}}{1+\left(\frac{[H^+]}{K_{D(E)}}\right)^{n}+\alpha_E}\right) \Big/ \left(\frac{1+\left(\frac{10^{-5}}{K_{D(E)}}\right)^{n}}{1+\left(\frac{10^{-5}}{K_{D(E)}}\right)^{n}+\alpha_E}\right) \quad (5)$$

To test this model, we designed several concatenated TALK1 mutant plasmids that express a single functional channel comprised of two different linked subunits. All the concatenated homodimeric channels, including WT-WT, R233A-R233A, and R233E-R233E showed pH_o sensitivities corresponding to those of dimers formed from plasmid-expressed single sequences (Fig. S6, *A*–*C*), suggesting the short linker did not affect the pH_o sensitivities. Since the order of coding sequences did not affect pH_o sensitivities (Fig. S6, *D*–*F*), we pooled the data from channels with the same combination (regardless of order) and used WT-R233A, WT-R233E, and R233E-R233A to represent three types of heterodimeric TALK1 channels.

Because TALK1 R233A is pH_o-insensitive, the dimeric channels containing one R233A subunit had the pH_o sensitivities dominated by the other subunit. Therefore, the pH_o sensitivities of WT-R233A and R233E-R233A could be predicted by Equations 1 and 5, respectively (Fig. 5, *B* and *C*). All parameter values used for predictions are listed in Table 1. Note that Equation 1 is normalized to pH_o 10, and Equation 5 is normalized to pH_o 5. These equations predict the augmentation of residual currents and shifting of $pK_{1/2}$. Indeed, the experimental results for WT-R233A and R233E-R233A corresponded well with these predictions (Fig. 5, *B* and *C*).

According to our hypothesis, the pH sensitivities of heterodimeric WT-R233E can be predicted by

$$P_{o(WT-E)} = P_{p(WT)} \times P_{p(E)} \quad (6)$$

For display as a relative pH_o sensitivity, Equation 6 was normalized to $P_{o\ (max)}$ using the parameters listed in Table 1. This equation predicts a U-shaped pH_o sensitivity curve for heterodimeric TALK1 WT-R233E, which corresponded well with our experimental results (Fig. 5*D*).

Discussion

TALK1 is an alkaline-activated K2P channel, and its activation is known to result from augmentation of open probability rather than single-channel conductance (33). Our results showed that the primary pH_o sensor of TALK1 is R233, and its alkaline activation can be modeled as an allosteric process. Moreover, we found that protonation of R233 impacts the C-type gate via an interaction network between R233, PH1, and SF. Our results imply that an interaction network between PH1 and SF supports a pore conformation that allows K^+ permeation. In an alkaline environment, deprotonated $R233^0$ does not perturb this network and an open channel conformation is maintained. In an acidic environment, however, protonated $R233^+$ could disturb the network of interactions among TM4, PH1, and SF (Fig. 3*A*) that destabilize the SF. Often, this disruption can induce the rotation of Ψ_{Y111} at the S1 binding site, causing Y111 to interact with L114, rendering the channel nonconductive.

The MD simulations suggested that R233, S97, and F100 are the critical residues for sensing pH_o. These residues form a pocket located between the extracellular space and the lipid bilayer, which is far away from SF. This pocket has been reported to serve as a detector for multiple physiological stimuli and regulates the C-type gates in other K2P channels; for

WT-R233A and R233E-R233A heterodimeric channels by fitting Equations 1 and 5, respectively, whereas the *red dots* are the experimental pH_o activation data for WT-R233A and R233E-R233A heterodimeric channels. *D*, the *blue line* represents predicted pH_o activation of WT-R233E heterodimeric channels by Equation 6, and the *blue dots* show the experimental pH_o activation data. TALK, TWIK-related alkaline pH-activated K+ channel.

example, it is involved in the activation of TREK1 and TREK2 by ML335, a K2P channel opener (22, 34), proton-induced inhibition of TASK2 and TALK2 (20, 28), and membrane-tension-sensing of TRAAK (14). Hence, this motif is considered as a common C-type gate regulation center for K2P channels. Our studies on TALK1-R233E also support the importance of this motif. A dication-mediated interaction between R233E and D94 inhibits channel activity, analogous to the interaction between $R233^+$ and PH1. Upon acidification or chelation of the divalent cations, this interaction is eliminated, and the TALK1-R233E channel returns to an open conformation. Interestingly, this inhibition appears to depend on the size of the divalent cation, as Ca^{2+} (ionic radius, 100 PM) is twice as potent as Mg^{2+} (ionic radius, 72 PM) (Fig. S4, *A–E*).

The flipping model we proposed for the TALK1 channel has not yet been observed in other K2P channels. Nevertheless, this model has been suggested for other potassium channels. In KcsA channels, the C-type inactivation is induced by disrupting the S1 and S3 potassium binding sites via flipping the carbonyl groups lining the SF. The glutamate at position 71 (E71) at the PH of KcsA channels serves as a pillar to support the SF by forming an extensive network of interactions with the neighboring residues (5, 6, 35). Mutating E71 to other noncharged residues disrupts this network and locks the carbonyl groups in place to prevent C-type inactivation (5, 6, 35). Solving the structures at various pH_o may provide high-resolution mechanistic insights into the C-type gating in TALK1 channels.

Heterodimeric K2P channels with different subtypes have been found in several tissues. These chimeric channels could exhibit the properties of the original subtype K2P channels in a hybrid activation pattern, such as those seen for heterodimeric TREK1-TREK2, TASK1-TASK3, THIK1-THIK2, TALK1-TASK2, and TALK1-TALK2 (23, 25, 36–38). In our model, the parameter α represents the ratio of conformational change in the C-type gate to the conformational change in the physiological sensor. Because the calculated value of α accurately predicts the behaviors of heterodimeric TALK1 channels, we suspect that this stochastic conformational change in sensor and C-type gate can explain the hybrid activation properties of heterodimeric K2P channels formed from different subtypes.

The Hill equation is widely used to describe how a macromolecule responds to ligands (39, 40). In this equation, the parameter $K_{1/2}$ represents the ligand concentration at which half response occurs. In the pH_o-gated channel, this parameter can be used to define the pH_o sensitivity (12). The equations we derived to describe the TALK1 kinetics are similar to the Hill equation; the relationship is given by

$$K_{1/2} = \left[\left(\frac{1}{1+\alpha}\right)^{1/n} K_d\right]^{-1}$$

for Equation 1 and

$$K_{1/2} = \left[\left(\frac{\sqrt{(2+\alpha^2)+\alpha^2}-\alpha}{(1+\alpha)(2+\alpha)}\right)^{1/n} K_d\right]^{-1}$$

for Equation 2. According to these relationships, the $K_{1/2}$ of Hill equation could be greatly affected by α, whether the channel has one or two pH_o-sensitive subunits. This implies that despite the same amino acid serving as the pH_o sensor in K2P channels of different subtypes, the gating range might vary according to α. Moreover, the parameter nH represents the cooperativity in ligand binding. When it is equal to 1, all receptors act independently, but when it is not equal to 1, the binding of a ligand to the first receptor subunit could positively or negatively affect the binding affinity of other receptor subunits (40). In our model, the parameter n is equivalent to nH. Theoretically, fitting the data with Equation 2 of the Hill equation suggested almost identical values for n and nH. The n value of TALK1-WT is lower than 1, indicating a negatively cooperative binding.

In conclusion, our study on the pH_o-gating mechanism of TALK1 not only expands the understanding of how physiological stimuli regulate C-type gate in K2P channels but also provides a functional model to explain the complex behaviors of the chimeric K2P channels. This gating model could offer a crucial molecular basis for understanding the actions of WT and disease-causing mutant K2P channels (29, 41, 42).

Experimental procedures

Plasmids

The pCDNA 3.1-human WT TALK1 variant 3 (NM_001135106) expression plasmid was a gift from Dr David A. Jacobson (Vanderbilt University). The pEXO-human TASK2 (NM_003740) was a gift from Dr Delphine Bichet (CNRS). Site-directed mutagenesis of the target plasmids was performed using the Quikchange strategy; primers were designed using the tool provided by Agilent Technologies (http://www.genomics.agilent.com/primerDesignProgram.jsp). The primers used to create TALK1 and TASK2 mutants are listed in Table S1. The sequences of the mutated clones were analyzed by an in-house sequencing facility (Sequencing Core, Institute of Biomedical Sciences, Academia Sinica). For experiments requiring heterodimeric or homodimeric tandem TALK1 mutant channels, we modified a method from a previous study (24). Briefly, the coding sequences of the first subunit (without stop codon) and second subunit were amplified by PCR. An amino acid linker Gly-Thr-Ala (GGTACCGCT) containing a KpnI restriction enzyme cutting site was added between the first and second sequences, and the whole sequence was ligated into the pCDNA 3.0 vector between the KpnI and XhoI restriction sites. The heterodimeric or homodimeric tandem channels were named as follows: subunit 1 and subunit 2, for example, WT (subunit 1)-WT (subunit 2).

Cell culture

COS-7 cells were maintained in Dulbecco's modified Eagle's medium (Gibco, 11966-025) supplemented with 10% fetal bovine serum in a humidified atmosphere of 5% CO2 at 37 °C. COS-7 cells were cotransfected with pN1-EGFP plasmid and target plasmid in a 1:9 ratio using PolyJet (SignaGen

Laboratories) transfection reagent. One day after transfection, GFP-expressing cells were selected for patch-clamp recording.

Electrophysiological recording

An Axon700B amplifier was used for patch-clamp experiments. The standard external solution contained 148 mM NaCl (Sigma, 31434), 2 mM KCl (Sigma, P3911), 1 mM $MgCl_2$ (Sigma, M2670), and 2 mM $CaCl_2$ (Sigma, C5080); pH was adjusted with NaOH or HCl. Various pH buffers were used to maintain the pH values: 10 mM 2-(N-morpholino)ethanesulfonic acid (Sigma, M3671) for pH 5.0, 2-[4-(2-hydroxyethyl) piperazin-1-yl]ethanesulfonic acid (Sigma, H4034) for pH 6.0 to 8.0, and N-(1,1-Dimethyl-2-hydroxyethyl)-3-amino-2-hydroxypropanesulfonic acid (Sigma, A6659) for pH larger than 9.0. The dication-free external solutions were made by omitting $MgCl_2$ and $CaCl_2$ and adding 1 mM EDTA to the standard external solution. The Ca^{2+} or Mg^{2+} external solutions were modifications of standard external solution with dications of only 1 mM $CaCl_2$ or 1 mM $MgCl_2$, respectively. Data were acquired at 10 kHz using the pCLAMP software (MolecularDevice). The electrodes were pulled from 1.5-mm borosilicate glass capillaries (Sutter Inc). Pipette resistances were 2 to 5 MΩ when filled with the intracellular solution containing 150 mM KCl, 10 mM 2-[4-(2-hydroxyethyl)piperazin-1-yl]ethanesulfonic acid, 5 mM EGTA, and 1 mM $MgCl_2$; pH was adjusted to 7.4 with KOH. The access resistances of whole-cell recording ranged between 5 and 20 MΩ and were compensated by 40 to 80%. All experiments were performed at room temperature (∼25 °C).

Modeling and MD simulations

The template structures of TASK2 at low (PDB ID: 6wlv) and high pH (PDB ID: 6wm0) were used for *de novo* structure predictions of WT TALK1 and various TALK1 mutants with Modeller 9.17 (43). The OPM database (44) was used to position the models respective to the membrane. The protonation states of the ionizable side chains respectively at pH 6.5 and 8.5 were determined using PROPKA3 (45). Missing hydrogen atoms were added using the HBUILD module in the CHARMM program (46) with the CHARMM36 forcefield (47). Each complex was then inserted into a POPC bilayer built using CHARMM-GUI (48). Once solvated with TIP3P (49) water molecules, the resulting system had a dimension of 100 × 100 × 127 Å (∼120,000 atoms), with 117 and 128 lipids in each leaflet, respectively. MD simulations were performed at a temperature of 310 K and 1 atm pressure using NAMD2.12 (50). All bonds to hydrogen atoms were constrained by the SHAKE algorithm (51). Long-range electrostatic forces were treated using the particle mesh Ewald method (52), with a grid spacing of 1 Å and a nonbond cutoff of 12 Å. First, the membrane-inserted system complex was minimized using 10,000 steps of conjugated gradient. Next, the system was equilibrated for 6 runs of 1 ns each, during which harmonic restraints on backbone and side chains were progressively lifted. An integration step of 1 fs was used in the first 3 runs, whereas 2 fs was used in the remaining rounds. For each complex built (dimer form), 10 independent replicates (replicate 1–10 for subunit 1 and replicate 11–20 for subunit 2) of a duration of 200 ns (unless stated otherwise) were generated (Table S2). Hydrogen bonds were analyzed using the CHARMM program (46) with an acceptor to hydrogen distance of ≤ 2.4 Å and a donor–hydrogen–acceptor angle of ≥ 130°. The simulation structures were visualized using Pymol.

Statistics

Electrophysiology Data were analyzed with pClamp10 software (Molecular Devices Corp.). Results are reported as means ± sd. Statistical analysis was performed using Prism 9 (Graph Pad), with differences considered significant at $p < 0.05$ ($^{*}p < 0.05$, $^{**}p < 0.01$, and $^{***}p < 0.001$). To calculate the effects of pH_0, the current measured at 0 mV in whole-cell recording was plotted against pH_o and fitted with the Hill equation: $I = I_{min} + (I_{max} - I_{min})/(1 + ([H^+]/K_{1/2})^{nH})$ or the TALK1 kinetic model (see Results and Fig. 5). To calculate the voltage activating time constant (τ), the current measured at a specific membrane potential was plotted against time and fitted with the equation, $f(t) = A\ (1 - e^{(-t/\tau)}) + C$. The fittings were made using Prism 9, pClamp10 or R software.

Data availability

All data are contained within the article and supporting information, or are available from the authors: Wen-Hao Tsai (howard1024@ibms.sinica.edu.tw) and Cédric Grauffel (cedric@ibms.sinica.edu.tw) upon request.

Supporting information—This article contains supporting information, Figs. S1–S6, Tables S1 and S2.

Acknowledgments—We thank Drs David A. Jacobson and Delphine Bichet for providing the K2P channel plasmids. We thank Dr Lily Y. Jan for the comments and suggestions. We thank Yvonne Hsu for her excellent technical support. We thank the outstanding support provided by Academia Sinica DNA sequencing Core Facility and Innovative Instrument Project (AS-CFII-108-115) and the Electrophysiology facility of the Institute of Biomedical Sciences, Academia Sinica.

Author contributions—W.-H. T., C. G., and S.-B. Y. conceptualization; W.-H. T., C. G., and S.-B. Y. methodology; W.-H. T., C. G., M.-Y. H., and S. P. investigation; W.-H. T. and S. P. formal analysis; W.-H. T., C. G., M. S. P., C. L., S.-B. Y. writing–original draft; W.-H. T., C. G., M.-Y. H., S. P., M. S. P., C. L., and S.-B. Y. writing–review and editing.

Funding and additional information—This work was supported by the Institute of Biomedical Sciences at Academia Sinica and the Ministry of Science and Technology, Taiwan (107-2923-B001-001-MY3, 106-2320-B-001-013 and 107-2320-B-001-026-MY3 to S. B. Y.).

Conflict of interest—The authors declare that they have no conflicts of interest with the contents of this article.

Abbreviations—The abbreviations used are: K2P, two-pore domain potassium channel; PH, pore helix; P_o, open probability; SF, selectivity filter; TALK, TWIK-related alkaline pH-activated K^+ channel; TASK, TWIK-related acid-sensitive K^+ channel; TM, transmembrane region; TREK, TWIK-related K^+ channel.

References

1. Zhou, Y., Morais-Cabral, J. H., Kaufman, A., and MacKinnon, R. (2001) Chemistry of ion coordination and hydration revealed by a K^+ channel-Fab complex at 2.0 A resolution. *Nature* **414**, 43–48
2. Lockless, S. W., Zhou, M., and MacKinnon, R. (2007) Structural and thermodynamic properties of selective ion binding in a K^+ channel. *PLoS Biol.* **5**, e121
3. Zhang, Y., Zhang, X., Liu, C., and Hu, C. (2021) Regulation of K(+) conductance by a hydrogen bond in Kv2.1, Kv2.2, and Kv1.2 channels. *Membranes (Basel)* **11**, 190
4. Miranda, W. E., DeMarco, K. R., Guo, J., Duff, H. J., Vorobyov, I., Clancy, C. E., *et al.* (2020) Selectivity filter modalities and rapid inactivation of the hERG1 channel. *Proc. Natl. Acad. Sci. U. S. A.* **117**, 2795–2804
5. Jekhmane, S., Medeiros-Silva, J., Li, J., Kummerer, F., Muller-Hermes, C., Baldus, M., *et al.* (2019) Shifts in the selectivity filter dynamics cause modal gating in K(+) channels. *Nat. Commun.* **10**, 123
6. Chakrapani, S., Cordero-Morales, J. F., Jogini, V., Pan, A. C., Cortes, D. M., Roux, B., *et al.* (2011) On the structural basis of modal gating behavior in K(+) channels. *Nat. Struct. Mol. Biol.* **18**, 67–74
7. Yang, Y., Yan, Y., and Sigworth, F. J. (1997) How does the W434F mutation block current in Shaker potassium channels? *J. Gen. Physiol.* **109**, 779–789
8. Pau, V., Zhou, Y., Ramu, Y., Xu, Y., and Lu, Z. (2017) Crystal structure of an inactivated mutant mammalian voltage-gated K^+ channel. *Nat. Struct. Mol. Biol.* **24**, 857–865
9. Han, J., Kang, D., and Kim, D. (2003) Functional properties of four splice variants of a human pancreatic tandem-pore K^+ channel, TALK-1. *Am. J. Physiol. Cell Physiol.* **285**, C529–538
10. Honore, E. (2007) The neuronal background K2P channels: focus on TREK1. *Nat. Rev. Neurosci.* **8**, 251–261
11. Sepulveda, F. V., Pablo Cid, L., Teulon, J., and Niemeyer, M. I. (2015) Molecular aspects of structure, gating, and physiology of pH-sensitive background K2P and Kir K^+-transport channels. *Physiol. Rev.* **95**, 179–217
12. Lesage, F., and Barhanin, J. (2011) Molecular physiology of pH-sensitive background K(2P) channels. *Physiology (Bethesda)* **26**, 424–437
13. Brohawn, S. G., del Mármol, J., and MacKinnon, R. (2012) Crystal structure of the human K2P TRAAK, a lipid- and mechano-sensitive K^+ ion channel. *Science* **335**, 436–441
14. Brohawn, S. G., Campbell, E. B., and MacKinnon, R. (2014) Physical mechanism for gating and mechanosensitivity of the human TRAAK K^+ channel. *Nature* **516**, 126–130
15. Brohawn, S. G., Su, Z., and MacKinnon, R. (2014) Mechanosensitivity is mediated directly by the lipid membrane in TRAAK and TREK1 K^+ channels. *Proc. Natl. Acad. Sci. U. S. A.* **111**, 3614–3619
16. McClenaghan, C., Schewe, M., Aryal, P., Carpenter, E. P., Baukrowitz, T., and Tucker, S. J. (2016) Polymodal activation of the TREK-2 K2P channel produces structurally distinct open states. *J. Gen. Physiol.* **147**, 497–505
17. Bagriantsev, S. N., Peyronnet, R., Clark, K. A., Honore, E., and Minor, D. L., Jr. (2011) Multiple modalities converge on a common gate to control K2P channel function. *EMBO J.* **30**, 3594–3606
18. Rajan, S., Wischmeyer, E., Xin Liu, G., Preisig-Muller, R., Daut, J., Karschin, A., *et al.* (2000) TASK-3, a novel tandem pore domain acid-sensitive K^+ channel. An extracellular histiding as pH sensor. *J. Biol. Chem.* **275**, 16650–16657
19. Sandoz, G., Douguet, D., Chatelain, F., Lazdunski, M., and Lesage, F. (2009) Extracellular acidification exerts opposite actions on TREK1 and TREK2 potassium channels *via* a single conserved histidine residue. *Proc. Natl. Acad. Sci. U. S. A.* **106**, 14628–14633
20. Niemeyer, M. I., González-Nilo, F. D., Zúñiga, L., González, W., Cid, L. P., and Sepúlveda, F. V. (2007) Neutralization of a single arginine residue gates open a two-pore domain, alkali-activated K^+ channel. *Proc. Natl. Acad. Sci. U. S. A.* **104**, 666–671
21. Brennecke, J. T., and de Groot, B. L. (2018) Mechanism of mechanosensitive gating of the TREK-2 potassium channel. *Biophys. J.* **114**, 1336–1343
22. Lolicato, M., Natale, A. M., Abderemane-Ali, F., Crottès, D., Capponi, S., Duman, R., *et al.* (2020) K(2P) channel C-type gating involves asymmetric selectivity filter order-disorder transitions. *Sci. Adv.* **6**, eabc9174
23. Levitz, J., Royal, P., Comoglio, Y., Wdziekonski, B., Schaub, S., Clemens, D. M., *et al.* (2016) Heterodimerization within the TREK channel subfamily produces a diverse family of highly regulated potassium channels. *Proc. Natl. Acad. Sci. U. S. A.* **113**, 4194–4199
24. Lengyel, M., Czirjak, G., and Enyedi, P. (2016) formation of functional heterodimers by TREK-1 and TREK-2 two-pore domain potassium channel subunits. *J. Biol. Chem.* **291**, 13649–13661
25. Blin, S., Ben Soussia, I., Kim, E. J., Brau, F., Kang, D., Lesage, F., *et al.* (2016) Mixing and matching TREK/TRAAK subunits generate heterodimeric K2P channels with unique properties. *Proc. Natl. Acad. Sci. U. S. A.* **113**, 4200–4205
26. Gonzalez, W., Zuniga, L., Cid, L. P., Arevalo, B., Niemeyer, M. I., and Sepulveda, F. V. (2013) An extracellular ion pathway plays a central role in the cooperative gating of a K(2P) K^+ channel by extracellular pH. *J. Biol. Chem.* **288**, 5984–5991
27. Niemeyer, M. I., Cid, L. P., Pena-Munzenmayer, G., and Sepulveda, F. V. (2010) Separate gating mechanisms mediate the regulation of K2P potassium channel TASK-2 by intra- and extracellular pH. *J. Biol. Chem.* **285**, 16467–16475
28. Li, B., Rietmeijer, R. A., and Brohawn, S. G. (2020) Structural basis for pH gating of the two-pore domain K(+) channel TASK2. *Nature* **586**, 457–462
29. Graff, S. M., Johnson, S. R., Leo, P. J., Dadi, P. K., Dickerson, M. T., Nakhe, A. Y., *et al.* (2021) A KCNK16 mutation causing TALK-1 gain of function is associated with maturity-onset diabetes of the young. *JCI Insight* **6**, e138057
30. Girard, C., Duprat, F., Terrenoire, C., Tinel, N., Fosset, M., Romey, G., *et al.* (2001) Genomic and functional characteristics of novel human pancreatic 2P domain K(+) channels. *Biochem. Biophys. Res. Commun.* **282**, 249–256
31. Schewe, M., Nematian-Ardestani, E., Sun, H., Musinszki, M., Cordeiro, S., Bucci, G., *et al.* (2016) A non-canonical voltage-sensing mechanism controls gating in K2P K(+) channels. *Cell* **164**, 937–949
32. Yuill, K. H., Stansfeld, P. J., Ashmole, I., Sutcliffe, M. J., and Stanfield, P. R. (2007) The selectivity, voltage-dependence and acid sensitivity of the tandem pore potassium channel TASK-1: contributions of the pore domains. *Pflugers Arch.* **455**, 333–348
33. Kang, D., and Kim, D. (2004) Single-channel properties and pH sensitivity of two-pore domain K^+ channels of the TALK family. *Biochem. Biophys. Res. Commun.* **315**, 836–844
34. Lolicato, M., Arrigoni, C., Mori, T., Sekioka, Y., Bryant, C., Clark, K. A., *et al.* (2017) K2P2.1 (TREK-1)-activator complexes reveal a cryptic selectivity filter binding site. *Nature* **547**, 364–368
35. Xu, Y., and McDermott, A. E. (2019) Inactivation in the potassium channel KcsA. *J. Struct. Biol. X* **3**, 100009
36. Blin, S., Chatelain, F. C., Feliciangeli, S., Kang, D., Lesage, F., and Bichet, D. (2014) Tandem pore domain halothane-inhibited K^+ channel subunits THIK1 and THIK2 assemble and form active channels. *J. Biol. Chem.* **289**, 28202–28212
37. Czirjak, G., and Enyedi, P. (2002) Formation of functional heterodimers between the TASK-1 and TASK-3 two-pore domain potassium channel subunits. *J. Biol. Chem.* **277**, 5426–5432
38. [preprint] Khoubza, L., Kim, E.-J., Chatelain, F. C., Feliciangeli, S., Kang, D., Lesage, F., *et al.* (2021) Heteromerization of alkaline-sensitive two-pore domain potassium channels. *bioRxiv*. https://doi.org/10.1101/2021.11.08.467666
39. Abeliovich, H. (2016) On Hill coefficients and subunit interaction energies. *J. Math. Biol.* **73**, 1399–1411
40. Qin, F. (2010) Hill coefficients of a polymodal Monod-Wyman-Changeux model for ion channel gating. *Biophys. J.* **99**, L29–31

41. Vierra, N. C., Dadi, P. K., Milian, S. C., Dickerson, M. T., Jordan, K. L., Gilon, P., *et al.* (2017) TALK-1 channels control beta cell endoplasmic reticulum Ca(2+) homeostasis. *Sci. Signal.* **10**, eaan2883
42. Vierra, N. C., Dadi, P. K., Jeong, I., Dickerson, M., Powell, D. R., and Jacobson, D. A. (2015) Type 2 diabetes-associated K+ channel TALK-1 modulates beta-cell electrical excitability, second-phase insulin secretion, and glucose homeostasis. *Diabetes* **64**, 3818–3828
43. Webb, B., and Sali, A. (2016) Comparative protein structure modeling using MODELLER. *Curr. Protoc. Bioinformatics* **54**, 5.6.1–5.6.37
44. Lomize, M. A., Pogozheva, I. D., Joo, H., Mosberg, H. I., and Lomize, A. L. (2012) OPM database and PPM web server: resources for positioning of proteins in membranes. *Nucl. Acids Res.* **40**, D370–376
45. Olsson, M. H. M., Søndergard, C. R., Rostkowski, M. R., and Jensen, J. H. (2011) PROPKA3: consistent treatment of internal and surface residues in empirical pKa predictions. *J. Chem. Theor. Comput.* **7**, 526–537
46. Brooks, B. R., Brooks, C. L., III, Mackerell, A. D., Nilsson, L., Petrella, R. J., Roux, B., *et al.* (2009) CHARMM: the biomolecular simulation program. *J. Comput. Chem.* **30**, 1545–1615
47. Huang, J., and MacKerell, A. D., Jr. (2013) CHARMM36 all-atom additive protein force field: validation based on comparison to NMR data. *J. Comput. Chem.* **34**, 2135–2145
48. Jo, S., Kim, T., Iyer Vidyashankara, G., and Im, W. (2008) CHARMM-GUI: a web-based graphical user interface for CHARMM. *J. Comput. Chem.* **29**, 1859–1865
49. Jorgensen, W. L., Chandrasekhar, J., Madura, J. D., Impey, R. W., and Klein, M. L. (1983) Comparison of simple potential functions for simulating liquid water. *J. Chem. Phys.* **79**, 926–935
50. Phillips, J. C., Braun, R., Wang, W., Gumbart, J., Tajkhorshid, E., Villa, E., *et al.* (2005) Scalable molecular dynamics with NAMD. *J. Comput. Chem.* **26**, 1781–1802
51. Andersen, H. C. (1983) RATTLE: a "velocity" version of the SHAKE algorithm for molecular dynamics calculations. *J. Comput. Phys.* **52**, 24–34
52. Essmann, U., Perera, L., Berkowitz, M. L., Darden, T., Lee, H., and Pedersen, L. G. (1995) A smooth particle mesh Ewald method. *J. Chem. Phys.* **103**, 8577–8592